Journal of Applied Fluid Mechanics, Vol. 11, No. 6, pp. 1591-1598, 2018.
Available online at www.jafmonline.net, ISSN 1735-3572, EISSN 1735-3645.
DOI: 10.29252/jafm.11.06.29141

Geometrical Optimization of an Inducer with Respect to Rotating Cavitation Generated Radial Forces by using an Orthogonal Experiment

L. Yu[1], H. C. Zhang[1], H. Chen[2], Y. P. Li[2], Z. G. Zuo[1†] and S. H. Liu[1]

[1] *State Key Laboratory of Hydroscience and Engineering Laboratory, Department of Energy and Power Engineering, Tsinghua University, Beijing, Beijing, 100084, China*
[2] *Xi'an Aerospace Propulsion Institute, Xi'an, Shanxi, 710100, China*

†*Corresponding Author Email: zhigangzuo200@mail.tsinghua.edu.cn*

(Received April 26, 2018; accepted July 3, 2018)

ABSTRACT

It is known that rotating cavitation (RC) characteristic of an inducer can greatly influence the safe and stable operation of a liquid rocket. In this paper, the possibility of geometrically optimizing an inducer with respect to RC generated radial forces was discussed. The characteristics of the inducer was firstly evaluated through computational fluid dynamics (CFD), which was validated against experimental results. Then by employing an orthogonal experiment combined with CFD, influences of geometric parametric combinations on RC were investigated. Primary influencing factors and the best parametric combination have been obtained through a variance analysis. Comparing with the original inducer, a significant improvement in the cavitation performance, as well as the radial force characteristic of the optimized inducer has been achieved. Pressure distribution on the blades have been analyzed to reveal the related flow mechanism. This work provides a feasible and effective route in engineering practice to optimize the characteristic of RC generated radial forces for an inducer.

Keywords: Inducer; Geometrical optimization; Orthogonal experiment; Rotating cavitation; Radial force characteristic.

NOMENCLATURE

C_p	pressure distribution coefficient	TE	trailing edge
c	tip clearance	l_t	the length of tip spiral expansion
F_x	x component of the radial force	l_h	the length of hub spiral expansion
Fy	y component of the radial force	R_h	the radius of spiral expansion at inducer hub
f_0	the rotational frequency	R_s	the radius of blade sweep
H	hydraulic head	R_t	the radius of spiral expansion at inducer tip
i	the number of levels	y_{ij}	the radial force value for factor j in level i
j	the number of factors	β_t	the blade angle at inducer tip
K	the variance between each factor	β_h	the blade angle at inducer hub
k	average value of each level for each factor	η	hydraulic efficiency
LE	leading edge	σ	Cavitation number $\sigma=(p_{in}-p_v)/0.5\rho\Omega^2 r_T^2$
N_i	the total number of levels	σ_b	Breakdown cavitation number
p_{in}	inlet static pressure	ρ	liquid density
p_v	vapor pressure	Ω	inducer rotational speed
r_T	inducer tip radius		

1. INTRODUCTION

As a key hydraulic component in liquid rocket engines, turbopumps are used to convey fuel and oxidizer to the combustor. Due to the requirement for a maximum power/weight ratio of the main pump, hence the persistent need for its weight reduction, the pump impeller always runs near the upper limit of the rotational speed, causing the possibility of cavitation development on the suction sides of the blades at the impeller inlet (d'Agostino, 2013; d'Agostino *et al.*, 2017). The occurrence of cavitation may lead to

pump performance degradation, i.e., a sharp decrease in head and efficiency, and large pressure fluctuations, i.e. hydraulic instabilities. To alleviate the influence of cavitation in the main pump impeller, an inducer is usually installed at its upstream. While cavitation occurrence is allowed in the inducer, instabilities caused by complex cavitating flows are often accompanied. Among them, rotating cavitation (RC), with complex unsteady flow and asymmetric cavity distribution, can induce significant radial forces to the impeller (Skelley, 2014; Tani, Yamanishi *et al.*, 2012; Zoladz, 2000), and is considered a major cause for the premature cutoff of the engines (Ryan *et al.*, 1994; Sekita, Watanabe *et al.*, 2001).

Therefore, efforts should be made in reducing/suppressing the effects of RC. Research show that the effects of RC can be effectively dampened by geometrical modification of the hydraulic domain of the inducer, e.g., casing modification (Hashimoto *et al.*, 1997; Fujii *et al.*, 2008, 2005; Shimiya *et al.*, 2008; Kang *et al.*, 2010), optimization of the inducer impeller, etc. Tsujimoto (2007) carried out experiments on five inducers with different leading edge sweep, and observed the suppression of RC in inducers with backward sweep through pressure fluctuation spectrum analysis. Kang, *et al.* (2009) demonstrated the experimental results of four inducers with different geometrical parameters (inlet tip blade angle and sweep angle, etc.) under different flow coefficients. It was found that for the inducer with a smaller inlet blade angle and a larger sweep, RC at the design and larger flow coefficients was avoided. Torre, *et al.* (2011) experimentally illustrated the influence of the tip clearance on RC on a three-bladed axial inducer. It was observed that the maximum amplitude of the pressure oscillation at the frequency of RC decreases with an increasing tip clearance. It can be concluded that all the geomertric optimization above were based on the study of a single factor, while physically RC can be affected by the synthetic influence of multiple factors. Additionally, pressure fluctuation was often used as an indication of RC in previous studies. However, in cavitating inducers, pressure sensor measurements are highly sensitive to installation positions of the sensors, with respect to the cavitation zone. From an engineering point of view, the radial force induced by the pressure distribution variation is a collective indication of the effects of RC on the bearing and shaft support structure, thus can be used for RC characteristic evaluation.

In this work, an orthogonal experiment combining numerical simulation has been employed to improve the RC characteristic in a three-bladed axial inducer. The characteristic of the radial force is chosen as an indication of RC. The influence of each geometric parameter has been obtained. Meanwhile, an optimized design with the best parametric combination is presented. Besides the improvement of cavitation performance, radial force characteristic and pressure distribution on the blades have been also greatly modified in the optimized inducer.

2. CASE STUDIED

The geometry of the three-bladed axial inducer impeller studied is shown in Fig. 1a. An annulus casing with a segregation board and a deflector (Fig. 1b) is positioned upstream of the inducer, in order to form a uniform inflow velocity distribution (Fei *et al.*, 2011). The CFD computational domain is shown in Fig. 2, including four hydraulic components: the inlet pipe, the annulus inlet casing, the inducer, and the outlet pipe. It is noted that the inlet pipe is extended 5 times the diameter of the annulus inlet casing, to obtain an unperturbed inlet flow in the simulations. The outlet pipe is extended 7 times the diameter of the inducer blade tip to ensure a fully developed outlet flow. Mass flow rate and pressure were chosen as the inlet and outlet boundary conditions respectively.

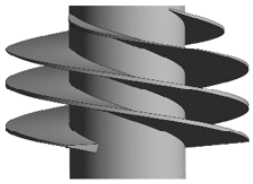

a)

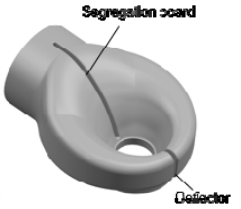

b)

Fig. 1. Geometry of a) the inducer impeller; b) the annulus casing.

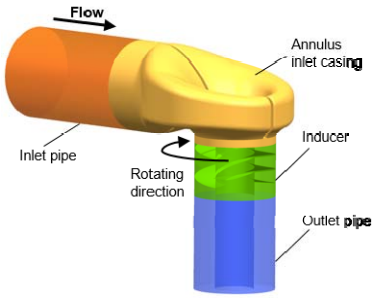

Fig. 2. Computational domain.

Three-dimensional computational fluid dynamic analyses were realized with the Multiple Reference Frame model in ANSYS CFX. The inducer impeller was set as a rotating domain with a rotational speed of 9 000r/min, and "no-slip" conditions were imposed on all solid boundary walls. RANS (Reynolds Averaged Navier-Stokes) equations were solved with SST $k-\omega$ turbulence model (Menter, 1994) and ZGB cavitation model (Zwart *et al.*, 2004). Steady flow calculations were carried out for the prediction of cavitation performances by setting a frozen-rotor interface between the annulus inlet casing and the inducer impeller. Unsteady numerical simulations were applied to evaluate the

characteristics of radial force fluctuations. The "transient rotor stator" was set between the rotating and stationary components for data transmission.

The computational mesh system of the entire hydrodynamic domain was developed in a commercial software package ANSYS ICEM. For the inlet and outlet pipes, hexahedral grids were chosen, while for the annulus inlet casing and the inducer, unstructured hybrid grids were utilized. Local grid refinements to the boundary layers in the inducer were applied to achieve the requirement (y^+<30) of SST $k-\omega$ turbulence model.

To find the best compromise between accuracy and computational time, a grid independence study was carried out firstly. Ten mesh systems with number of grids varying from 1.57×10^6 to 9.8×10^6 were chosen. Figure 3 shows the obtained hydraulic head (H) and efficiency (η). It is seen that when the number of grids reaches 3.52×10^6, the increase of the number of grids has little effect on the hydraulic head and efficiency. Considering the demand of the precise capturing of the frequency characteristics of the radial force fluctuations, the mesh system with 6.9×10^6 elements was used for subsequent calculations.

For unsteady simulations, time independence tests were performed to choose a proper time step size. As shown in Fig. 4, FFT analyses on the radial force of a certain blade were carried out against two different time step sizes (corresponding to 1° and 2° of the inducer impeller rotations, respectively). The peak characteristic was captured in both calculations with only a mild difference in the peak value of the fluctuation amplitude. Considering the computational accuracy and calculation loads, the time step when the inducer rotates 2° was chosen for the following unsteady flow simulations.

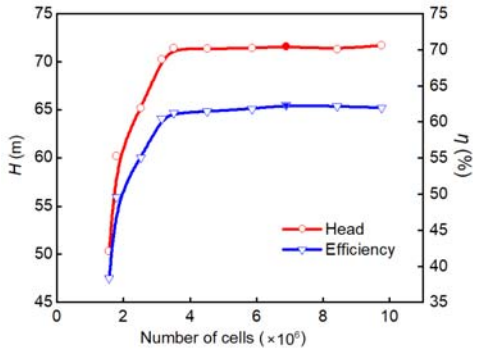

Fig. 3. Grid independence verification with respect to hydraulic head and efficiency.

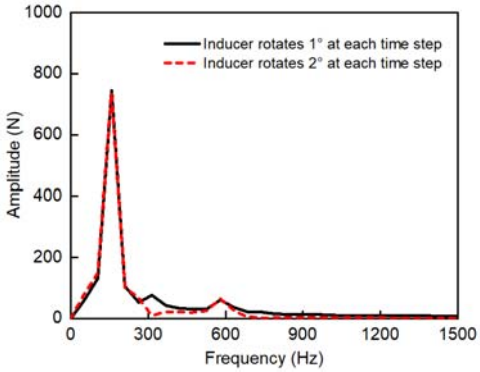

Fig. 4. Verification of time independence, FFT results of the radial force at tested time step sizes.

3. THE ORTHOGONAL EXPERIMENT

Employing orthogonal experiment is an effective optimization method to achieve target with multiple factors and levels. It is used to find the optimal scheme as well as minimizing the number of test runs (Karna *et al.*, 2012), and has been successfully applied in geometrical optimization of pump impellers (Ji *et al*.,2017; Ling *et al*.,2013). The basic steps of an orthogonal experiment are as follow:

Step 1. Determine test index

In this study, radial force was selected as an indication of RC.

Step 2. Select geometric factors and levels

Based on previous design experience, four important geometrical factors were selected, namely, the shape of tip spiral l_t, the shape of hub spiral l_h, the radius of blade sweep R_s, and the tip clearance c.

Factor A: the shape of tip spiral expansion (l_t)

The original inducer is a flat-plate inducer with a straight tip and hub spiral expansion line. While for optimal ones, arc lines are selected (as in Fig. 5). The radius of arc lines can be calculated by $R = l_0 / 2\sin\left(\dfrac{\beta_t - \beta_h}{2}\right)$.

Level 1: R_{t1} ($\beta_{t2} - \beta_{t1} = 1°$)

Level 2: R_{t2} ($\beta_{t2} - \beta_{t1} = 2°$)

Level 3: R_{t3} ($\beta_{t2} - \beta_{t1} = 3°$)

Factor B: the shape of hub spiral expansion (l_h)

Level 1: R_{h1} ($\beta_{h2} - \beta_{h1} = 1°$)

Level 2: R_{h2} ($\beta_{h2} - \beta_{h1} = 2°$)

Level 3: R_{h3} ($\beta_{h2} - \beta_{h1} = 3°$)

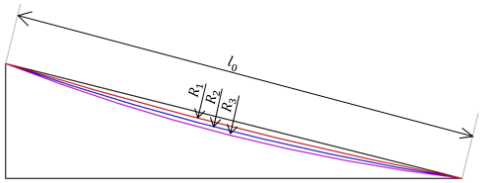

Fig. 5. Schematic of spiral expansion lines.

Factor C: the radius of blade sweep (R_s)

Level 1: $R_{s1} = R_{s0} + 3mm$

Level 2: $R_{s2} = R_{s0} + 3mm$

Level 3: $R_{s3} = R_{s0} + 3mm$

Factor D: tip clearance (c)

Level 1: 1.5 c_0

Level 2: 1.8 c_0

Level 3: 2.0 c_0

Step 3. Arrange the orthogonal array

The orthogonal table is used to arrange the experiments. Four factors are evaluated each time, and each factor takes three levels, as presented in Table 1.

Step 4. Carry out the test

Step 5. Analyze the results and find out the primary factors and levels

Table 1 Detailed experimental programs

Models	A	B	C	D
I	1	1	1	1
II	1	2	2	2
III	1	3	3	3
IV	2	1	2	3
V	2	2	3	1
VI	2	3	1	2
VII	3	1	3	2
VIII	3	2	1	3
IX	3	3	2	1

4. RESULTS AND DISCUSSIONS

4.1 Validation of the Numerical Methods

Comparisons between calculated and experimental results of the original inducer are carried out for the validation of the numerical methods. Two radial force components (F_x and F_y) with a phase difference of 90° were monitored. Figure 6 shows the FFT analyses of F_x and F_y. The frequency corresponds to the maximum amplitude of the two components is 158 Hz (1.05 times the rotational frequency f_0=150 Hz). Comparing to the experimental 1.13 f_0 (Hui *et al*, 2009), it can be seen that the numerical methods could reasonably simulate the RC generated radial forces in this inducer.

4.2 Results of the Original Inducer (Model O)

The cavitation performance of Model O is illustrated in Fig. 7. It can be observed that a breakdown of the head and efficiency occurs when the cavitation number $\sigma=(p_{in}-p_v)/0.5\rho\Omega^2r_T^2$ is lower than 0.017 (breakdown cavitation number σ_b, at which major deterioration in the performance occurs), i.e., the inlet pressure is lower than 0.06MPa. At the conditions of $\sigma > \sigma_b$, the head and efficiency remain almost unchanged.

The radial force characteristics of Model O were monitored in unsteady simulations under the design condition. Figure 8 shows the time series and FFT analysis of the radial force magnitude. The average radial force magnitude was obtained from time series analysis, with a value of 697N. And the FFT result shows that the maximum amplitude of radial force is 196N, with a corresponding frequency 158 Hz (~1.05 f_0). A lower amplitude of 66N at 448Hz (~3 f_0) caused by the blade rotation was also observed.

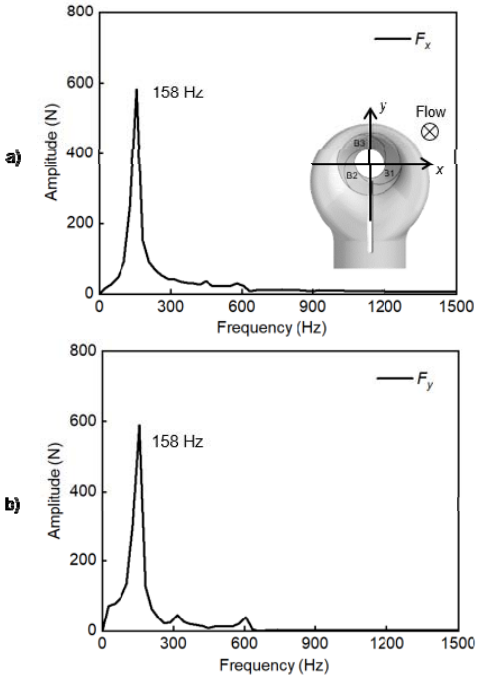

Fig. 6. FFT results on the two components of the radial force.

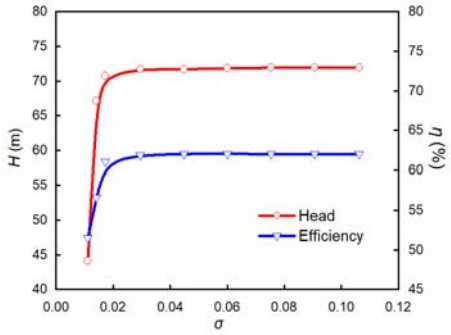

Fig. 7. Cavitation performance of Model O.

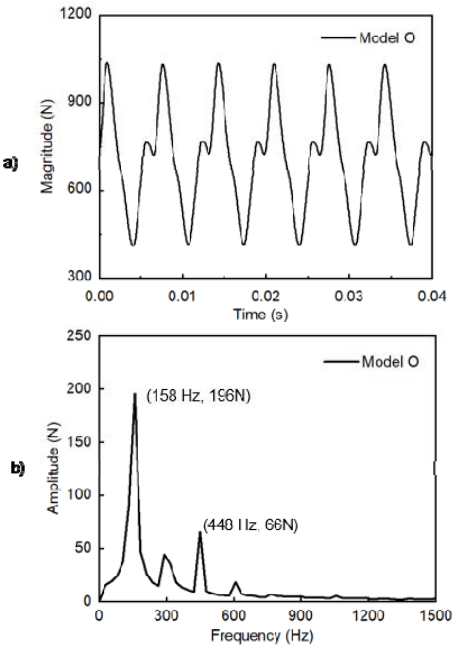

Fig. 8. Radial force characteristics of Model O. a) Time series; b) FFT analysis.

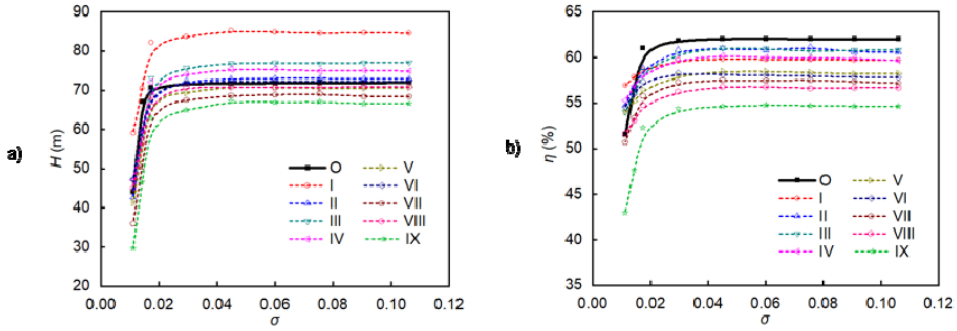

Fig. 9. Cavitation performance of Model O and modified models. a) Head; b) Efficiency.

4.3 Results of the Orthogonal Experiment

The cavitation performance of Model O and modified models (Model I~IX) are illustrated in Fig. 9. It can be found that Model I, II, III, IV and VI have an improved head performance at cavitation number $\sigma>\sigma_b$, while the efficiency of all the modified models is lower than that of Model O at $\sigma>\sigma_b$.

The radial force characteristics of the modified models were also monitored in unsteady simulations under the design condition. Table 2 lists the average radial force magnitudes and the FFT analysis results. It is seen that except for Model V, the average magnitudes of all the other modified models are larger than Model O. Additionally, FFT results of all the modified models have a frequency component of 158Hz, and the corresponding amplitudes of Model II, IV, VI and VII are lower than Model O.

Table 2 Characteristics of the radial force in Model O and modified models

Model	Parameters				Average (N)	Amplitude at 158 Hz (N)
	A	B	C	D		
O	0	0	0	0	697	196
I	1	1	1	1	959	517
II	1	2	2	2	727	142
III	1	3	3	3	714	198
IV	2	1	2	3	726	176
V	2	2	3	1	692	231
VI	2	3	1	2	738	158
VII	3	1	3	2	698	160
VIII	3	2	1	3	825	438
IX	3	3	2	1	808	261

To identify the influence of the main parameters on the objective index, a variance analysis is applied. The average value of each level for each factor is defined as k, and the variance between each factor is defined as K to analyze the difference between the maximal and minimal value of the four levels for each factor. Therefore, k and K can be calculated as follow:

$$k_i=\frac{1}{N_i}\sum_{i=1}^{N_i} y_{ij}$$

$$K=\max[k_1,k_2,...]-\min[k_1,k_2,...]$$

Where i is the number of levels, j is the number of factors, y_{ij} is the radial force value for factor j in level i, and Ni is the total number of levels. In this study, Ni =3.

The analysis results are shown in Table 3. According to the values of K, the factor influence rank of the average radial force is C>D>A>B, i.e., the radius of blade sweep is the most important factor. Accordingly, the best combination of parameters is A2, B2, C3, and D2. While for the amplitude at 158Hz, the rank is D>C>A>B. Thus, the primary factor that impacts the amplitude at 158Hz is the tip clearance. The best model for a lower amplitude is A2, B3, C2, and D2.

Table 3 Range analysis of average radial force and amplitude at 158Hz

Levels	Average radial force (N)				Amplitude at 158Hz (N)			
	A	B	C	D	A	B	C	D
k_1	800	794	841	820	286	284	371	336
k_2	719	748	754	721	188	270	193	153
k_3	777	753	701	755	286	206	196	271
K	81	46	140	99	98	78	178	183
Rank	3	4	1	2	3	4	2	1

4.4 Final Optimization (Model N)

In the present study, fluctuation characteristic of the radial force is of interest, so the optimized inducer design was adopted as A2, B3, C2, and D2. It is designed and simulated using the aforementioned method. Figure 10 shows the comparison of the predicted performance between Model O and Model N. It can be seen that both the head and the efficiency of Model N have been greatly improved. At the design condition (σ=0.075), Model N has an efficiency of 67% and a head of 84.1m, increased by 8% and 17% respectively, comparing with Model O (62%, 71.9m).

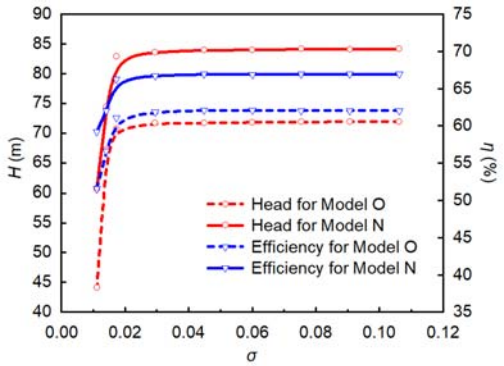

Fig. 10. Performance comparison.

The orbits of the radial force in 9 Rev. is depicted in Fig. 11. Compared to Model O, Model N has a more uniform radial force distribution with a smaller magnitude in most conditions. Comparison of the time series and

frequency domain results of the force magnitude are shown in Table 4 and Fig. 12. Besides the average magnitude and the amplitudes of FFT results, the standard deviation, indicating the difference of instantaneous value and the average, is also analyzed. A 14% decrease of the average magnitude can be observed. The standard deviation of the magnitude of Model N is 17N, which is much lower than that of Model O (174N), indicating a much smaller variation range of the instantaneous radial force. As for the FFT analysis, it can be seen that the amplitudes at both 158Hz and 448Hz are lower for Model N. In contrast to Model O, the 1st main frequency of Model N is 448Hz (~ 3 f_0), showing that the main impact factor under this circumstances is the rotation of the inducer, and the influence of RC on radial force fluctuation is smaller.

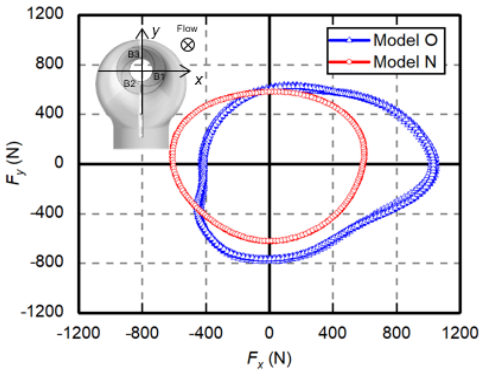

Fig. 11. Orbits of the radial force.

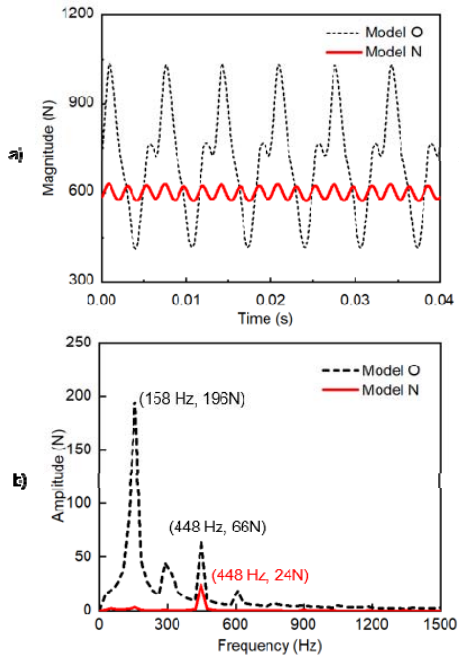

Fig. 12. Comparison of time series and frequency domain analysis results. a) Time series; b) FFT analysis.

To further understand the radial force characteristic, pressure distribution on the suction side (S) and pressure side (P) of the three blades at different spans (30%, 60%, and 90%) were analyzed. When the pressure on the pressure side is higher than that on the suction side, the blades exert work to the liquid, affecting the head of the inducer. The pressure difference between the pressure and suction side, and the uniformity of pressure distribution on each blade will influence the load on the inducer. Figure 13 shows a typical result of Model O. It is seen that the pressure distribution trends of the three blades (B1, B2, and B3) at 30% span and 60% span (without cavity along the trajectory from leading edge to trailing edge) are quite similar, while the trend at 90% span (with cavities near the leading edge) is different. Similar conclusion can be obtained in Model N. Therefore, the pressure distribution at 90% span is emphasized in the following analysis.

Table 4 Range Comparison of the radial force characteristic

Model	Average (N)	Standard deviation (N)	Amplitude at 158Hz (N)	Amplitude at 448Hz (N)
O	697	174	196	66
N	598	71	4	24

Figure 14 shows the pressure distributions of the three blades at 90% span and the corresponding vapor volume fraction contours of Model O at different time. Intersection of the pressure side and the suction side curve can be seen in all cases, indicating that only part of the blade can generate head. For the cases with larger radial force magnitudes (O1>O2 ≈ O3>O4), more unevenly distributed pressure between blades a greater maximum pressure coefficient occur. For the cases with a similar radial force magnitude (O2 and O3), the unevenness of pressure distribution in the three blade is similar. However, for O2 case, the maximum pressure coefficient was found on B2, while it appears on B3 for O3 case, resulting in a difference of the force direction between the two cases. The vapor volume fraction contours reveal that the cavitation volume of the three blades are different, which is the main reason for the uneven pressure distribution.

For Model N (as demonstrated in Fig. 15), no intersection can be found on all the blades. And a persistent positive pressure difference between the suction and pressure sides from leading edge to trailing edge generates a higher head, as illustrated in Fig. 10. A same relationship between the radial force magnitude and the pressure distribution in Model N can be found. The larger the radial force magnitude (N1>N2≈N3>N4), the less uniform the pressure distribution. For the cases with a similar magnitude (N2 and N3), the pressure distribution tends to be similar, but the maximum pressure coefficient appears on a different blade, leading to a different force direction. The vapor volume fraction contours show that the cavity areas of Model N is smaller and more evenly distributed than Model O.

5. CONCLUSIONS

To evaluate the geometrical influences on RC generated radial forces, an orthogonal experiment combining with the numerical simulation was employed in the present study. The numerical simulation result of the original inducer (Model O) agrees well with the experimental results, and the characteristics of RC can be effectively captured with the selected numerical methods. According to the orthogonal table, 9 inducers were designed and modeled. Through a variance analysis, the primary influencing factors have been determined, i.e., the tip clearance and the radius of blade sweep.

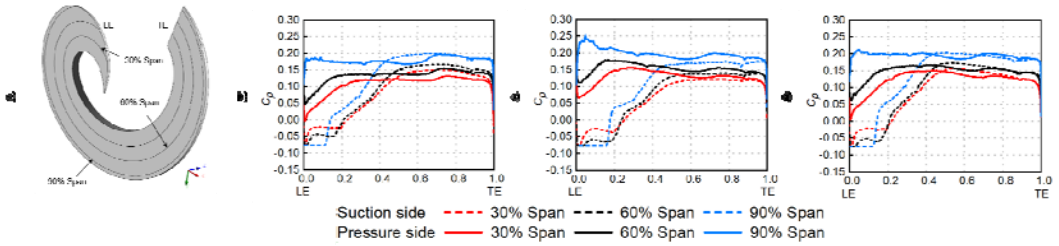

Fig. 13. A typical result of pressure distribution of Model O. a) Pressure distribution on B1; b) Pressure distribution on B2; c) Pressure distribution on B3; d) Schematic of pressure measuring lines.

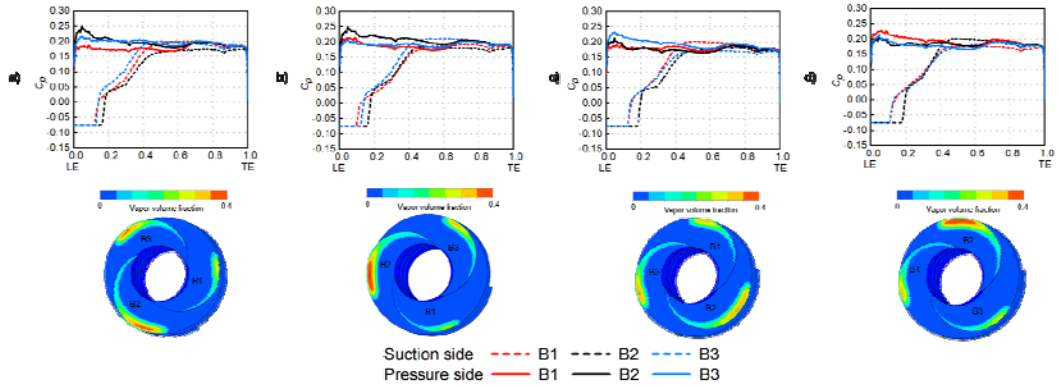

Fig. 14. Pressure distribution at 90% span and vapor volume fraction contour of Model O at different time.
a) Results for the case with maximum radial force (O1); b) Results for the case with medium radial force (O2);
c) Results for the case with similar radial force magnitude as O2 (O3); d) Results for the case with minimum radial force (O4).

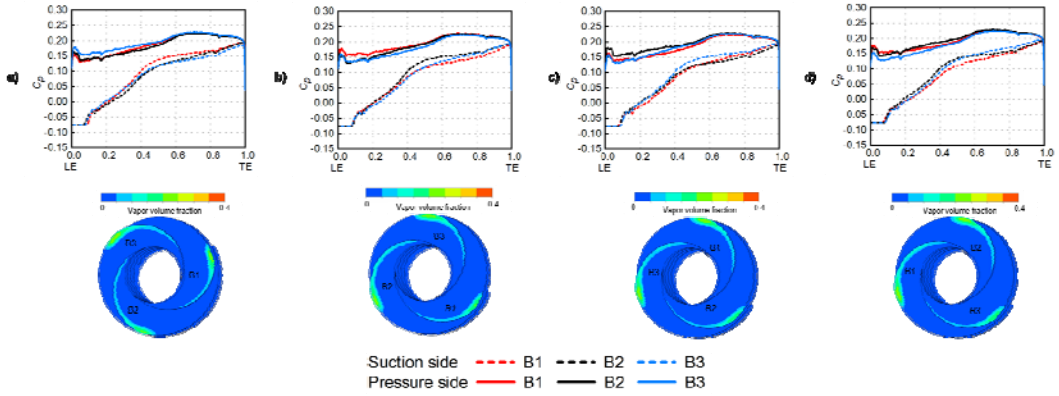

Fig. 15. Pressure distribution at 90% span and vapor volume fraction contour of Model N at different time.
a) Results for the case with maximum radial force (N1); b) Results for the case with medium radial force (N2);
c) Results for the case with similar radial force magnitude as O2 (N3); d) Results for the case with minimum radial force (N4).

Meanwhile, an optimized inducer (Model N) with a more uniform radial force distribution was obtained. The magnitude of its radial force is smaller in most cases. Its amplitudes at both 158Hz (the frequency of fluctuation induced by RC) and 448Hz (the blade passing frequency induced by the rotation of the inducer) are lower than Model O. In contrast to Model O, the 1st main frequency of the optimal inducer is 448Hz, indicating a smaller impact of RC on the radial force fluctuation. In addition, the pressure distribution and the cavity distribution on the blades are greatly improved in Model N, resulting in the improvement of cavitation performance and the radial force characteristic.

ACKNOWLEDGEMENTS

The authors would like to thank the National Basic Research Program of China ("973" Project) (Grant No. 613321) and the State Key Laboratory of Hydroscience and Engineering, Tsinghua University (Grant No.2017-KY-03) for their financial supports.

REFERENCES

d'Agostino, L. (2013, April). Turbomachinery developments and cavitation. In *VKI Lecture Series on Fluid Dynamics Associated to Launcher Developments, von Karman Institute of Fluid Dynamics,* Rhode-Saint-Genese, Belgium.

d'Agostino, L., A. Cervone, L. Torre, G. Pace, D. Valentini and A. Pasini (2017). An Introduction to Flow-Induced Instabilities in Rocket Engine Inducers and Turbopumps. In L. d'Agostino & M. V. Salvetti (Ed.), *Cavitation Instabilities and Rotordynamic Effects in Turbopumps and Hydroturbines: Turbopump and Inducer Cavitation, Experiments and Design*, 65-86. Cham: Springer International Publishing.

Fei, T., L. Jiawen, C. Hui, L. Xiangyang and X. Tong (2011). Study on Cavitation Performance of Inducer with Annulus Inlet Casing. *Journal of Mechanical Engineering* 47(4), 171-176.

Fujii, A., S. Mizuno, H. Horiguchi and Y. Tsujimoto (2005). Suppression of Unsteady Cavitation by Jet Injection at Inducer Inlet. *Transactions of the Japan Society of Mechanical Engineers Series B* 71(707), 1829-1838.

Fujii, A., S. Mizuno, H. Horiguchi and Y. Tsujimoto (2008). A Method for the Suppression of Rotating Cavitation by an Accumulator at the Inlet of an Inducer. *Journal of Fluid Science and Technology* 3(7), 838-845.

Hashimoto, T., H. Yamada, S. Funatsu, J. Ishimoto, K. Kamijo and Y. Tsujimoto (1997, July). Rotating cavitation in three and four-bladed inducers. In *33rd Joint Propulsion Conference and Exhibit*. Seattle, U.S.A.

Hui, C., L. Bin, Z. Enzhao and T. Yonghua (2009). Rotating cavitation of high-speed rotational inducer of LPRE *Journal of Propulsion Technology* 30(4), 390-395.

Ji, P., Y. Tingyun, Y. Shouqi and W. Wenjie (2017). Cavitation Optimization for a Centrifugal Pump Impeller by Using Orthogonal Design of Experiment. *Chinese Journal of Mechanical Engineering* 30(1), 103-109.

Kang, D., Y. Arimoto, K. Yonezawa, H. Horiguchi, Y. Kawata, C. Hah and Y. Tsujimoto (2010). Suppression of Cavitation Instabilities in an Inducer by Circumferential Groove and Explanation of Higher Frequency Components. *International Journal of Fluid Machinery and Systems* 3(2), 137-149.

Kang, D., T. Watanabe, K. Yonezawa, H. Horiguchi, Y. Kawata and Y. Tsujimoto (2009). Inducer Design to Avoid Cavitation Instabilities. *International Journal of Fluid Machinery and Systems* 2(4), 439-448.

Karna, S. K. and R. Sahai (2012). An overview on Taguchi method. *International Journal of Engineering and Mathematical Sciences* 1(1), 1-7.

Ling Z., S. Weidong, W. Suqing (2013). Performance optimization in a centrifugal pump impeller by orthogonal experiment and numerical simulation.Advances in Mechanical Engineering 2013, 385809

Menter, F. R. (1994). Two-equation eddy-viscosity turbulence models for engineering applications. *AIAA Journal* 32(8), 1598-1605.

Ryan, R., L. Gross, D. Mills and P. Mitchell (1994, June). The Space Shuttle Main Engine liquid oxygen pump high-synchronous vibration issue, the problem, the resolution approach, the solution. In *30th Joint Pro-pulsion Conference and Exhibit*. Indianapolis, U.S.A.

Sekita, R., A. Watanabe, K. Hirata and T. Imoto (2001). Lessons learned from H-2 failure and enhancement of H-2A project. *Acta Astro-nautica* 48(5), 431-438.

Shimiya, N., A. Fujii, H. Horiguchi, M. Uchiumi, J. Kurokawa and Y. Tsujimoto (2008). Suppression of Cavitation Instabilities in an Inducer by J Groove. *Journal of Fluids Engineering* 130(2), 021302-021302-7.

Skelley, S. (2014, January). Rotating Balances used for Fluid Pump Testing. In *52nd AIAA Aerospace Sciences Meeting*, National Harbor, Maryland.

Tani, N., N. Yamanishi and Y. Tsujimoto (2012). Influence of Flow Coefficient and Flow Structure on Rotational Cavitation in Inducer. *Journal of Fluids Engineering-Transactions of the Asme* 134(2), 021302-021302-13.

Torre, L., A. Pasini, A. Cervone, G. Pace, P. Miloro and L. D'Agostino (2011). Effect of Tip Clearance on the Performance of a Three-Bladed Axial Inducer. *Journal of Propulsion and Power* 27(4), 890-898.

Tsujimoto, Y (2007). Suppression of cavitation instabilities. In L. d'Agostino & M. V. Salvetti (Ed.),Fluid dynamics of cavitation and cavitating turbopumps, Italy, 211-229. SpringWienNewYork

Zoladz, T. (2000, January). Observations on rotating cavitation and cavitation surge from the development of the Fastrac engine turbopump. In *36th AIAA/ASME/SAE/ASEE Joint Propulsion Conference and Exhibit, Joint Propulsion Conferences*, Huntsvill, Alabama

Zwart, P. J., A. G. Gerber and T. Belamri (2004, May). A two-phase flow model for predicting cavitation dynamics. In *5th international conference on multiphase flow,* Yokohama, Japan.